Numerical Methods in Civil Engineering

# Stability Analysis of Rocking Soil-Structure Systems Subjected to Near-Fault Pulses

**Masoud Ahmadi* and Hamid Masaeli****

*ARTICLE INFO*

*Article history:*
*Received:*
*June 2020.*
*Revised:*
*August 2020.*
*Accepted:*
*September 2020.*

*Keywords:*
*Stability Analysis;*
*Overturning Uplifting;*
*Near-Fault Pulse;*
*Forward Rupture Directivity;*
*Fling Step.*

***Abstract:***

*The overturning potential of rocking soil-structure systems subjected to near-fault pulses is investigated in this paper. An extensive parametric study is conducted, including medium-to-high-rise buildings with different aspect ratios based on shallow raft foundation allowed to uplift considering the effects of nonlinear soil-structure interaction. The considered parameters are (i) ground motion characteristics, (ii) structural properties of the superstructure, and (iii) foundation design parameters. Mathematical directivity and fling pulses are used as input ground motion. The superstructure is assumed to predominantly showcase first-mode characteristics. Two-dimensional overturning spectra of buildings of various geometrical, as well as dynamic characteristics, are derived. Evidently, the prevalent pulse period ($T_p$) is a key parameter governing the rocking response of the system. It is also observed that fling pulses are more destructive than directivity pulses of the same magnitude with respect to overturning potential. On the other hand, the lower frequency parameter (p) of the more large-size buildings is a quantity that indicates higher safety margins against toppling with respect to small-size buildings of the same aspect ratio.*

## 1. Introduction

A significant amount of research in recent years is devoted to evaluating the effects of near-fault ground motions on structural and geotechnical systems. Especially after Northridge, Kobe, Kocaeli, and Chi-Chi earthquakes, two salient features of near-fault ground motions, namely "forward directivity" and "fling step", have become more of interest to researchers. Forward rupture directivity emerges as a single long-period high-amplitude pulse occurring near the beginning of shaking and is oriented perpendicularly to the fault [1]. The fling-step effect is the outcome of the permanent tectonic deformation of the earth in the proximity of the fault. It manifests itself in the record with a static residual displacement, observed in the strike-parallel and strike-normal directions for strike-slip and dip-slip faults, respectively [2,3].

* *Corresponding Author: Assistant Professor, Department of Civil Engineering, Ayatollah Boroujerdi University, Boroujerd, Iran, Email: masoud.ahmadi@abru.ac.ir.*

** *Assistant Professor, Department of Civil Engineering, Ayatollah Boroujerdi University, Boroujerd, Iran.*

Assessing the potential of near-fault pulses that bring about damage in structures, was first initiated by Bertero [4]. Thereafter this trend was followed by several investigations on seismic performance of various structural and geotechnical systems subjected to near-fault ground motions. Some of these studies have given particular attention to the potentially destructive effects of directivity and fling pulses using a mathematical representation of these two phenomena [5–13].

In the meantime, the inevitable inclusion of soil-structure interaction (SSI) under the influence of strong near-fault ground motions, has turned attention to elaborating on soil-structure response and potential vulnerability to directivity and fling pulses. Spyrakos and Nikolettos [14] proposed novel criteria for overturning the stability of flexible structures. They attempted to develop a simple design criterion that includes flexibility effects of slender structures to their overturning stability. They addressed the inverse problem to estimate the ground acceleration that caused the toppling of a slender structure. Zhang and Tang [15] studied the inertial SSI effects on linear and bilinear structures supported on the foundation that are able to translate and

rock when subjected to mathematical near-fault pulses. Acikgoz and DeJong [16] addressed the fundamental dynamics of flexible rocking structures with an analytical approach. They compared the rocking response of flexible structures with those of similar linear elastic oscillators and rigid rocking structures, revealing the distinct characteristics of flexible rocking structures. Peng et al. [17] proposed a simple analytical method to predict the overturning loads for single-column pier bridges. Their novel approach provided an iterative method that could determine the minimum critical load patterns at which an overturning state was reached. Haeri and Fathi [18] studied the rocking behavior of shallow foundations subjected to slow cyclic loading with the consideration of SSI. They concluded that deploying the linear elastic-perfect plastic approach may result in higher uplift of the foundation in comparison to that using a non-linear elasto-plastic approach, particularly in structures with lower heights. Jia et al. [19] performed stability analyses of blocky structure system using discontinuity layout optimization (DLO). Their proposed DLO procedure was extended to mimic rotations in the approximate simulation of rotational and translational failures along boundaries, thus simulating the mechanism on the rotating block. Their results demonstrated that the DLO was a simple but scientific method for identifying the mechanism of the critical failure of blocky structures.

In particular, the effect of elasticity on uplift, overturning instability, and harmonic response, from which an uplifted resonance emerges, was also investigated.

Regarding recent findings on seismic performance evaluation of soil-structure systems subjected to near-fault ground motions, it would be a promising idea to incorporate foundation uplifting in the problem. Accordingly, the work presented here aims to elaborate on the role of rocking-induced nonlinear effects of SSI during low-frequency high-amplitude excitation of directivity and fling pulses. To this end, an extensive parametric study is conducted. Medium-to-high-rise building structures with different aspect ratios based on shallow raft foundation are investigated. Mathematical directivity and fling pulses are used as input ground motion. The superstructure is assumed to predominantly showcase first-mode characteristics. The comparative assessments provide further insight into the soil-foundation-structure interaction problem considering nonlinear effects of foundation uplifting. In addition, the stability analysis of the rigid-block-on-rigid-base model due to overturning potential is discussed.

## 2. Overturning Potential of Rocking Structures

Evaluation of overturning potential of rocking structures necessitates advanced soil-structure interaction analysis and a huge amount of computational efforts, which is an inappropriate procedure for common applications. Therefore, as shown in Fig. 1, it is attempted to further simplify the rocking structure with the surface foundation of width $B$ as a rigid block of the same width, rocking on a rigid base (Fig. 1c). The issue of earthquake-induced rocking of rigid blocks on rigid base has been studied very thoroughly over the last decades (e.g. [20–24]), revealing the sensitive and highly nonlinear nature of the problem.

The rigid-block approximation inherently implies three fundamental assumptions [25]: (i) The rigid block assumption ignores the flexibility of the system. However, past studies postulate that the effect of system flexibility is negligible since the behavior is rocking-dominated and bending is minimal. (ii) The possible contribution of higher modes of vibration (for mdof structures) is ignored. Yet, according to Bielak [26], who investigated the response of fixed-base systems, the contributions of the second and higher modes to the overturning moment at the base of any classical linear system whose fundamental mode is given by a straight line, vanish identically. (iii) The rigid base assumption makes it impossible to capture the effect of soil compliance. Based on these assumptions, the rigid-block approximation estimates a conservative upper-bound of earthquake displacement demand for which the rocking building survives (toppling will not take place). Accordingly, in the present study, an analytical approach is conducted for a rigid block on a rigid base subjected to mathematical directivity and fling pulses.

## 3. Rigid-Block-on-Rigid-Base System Description

According to Fig. 1, the primary system can be modeled by the symmetric rigid block of mass $m$ and centroid mass moment of inertia $I$, (Fig. 1c). The rigid block of height $H=2h$, and width $B=2b$ is assumed to rotate about the corners O and O'. The distance between one corner of its base and the mass center is denoted by $r$, and the angle measured between $r$ and the vertical axis when the body is at rest is denoted by $\alpha$, where $\alpha = \tan^{-1}(h/b)$.

The system's dynamic response is realized by permitting the block to pivot on its corners with respect to the horizontally-moving base. The system then is a rigid 1-dof oscillator. Sliding of the block relative to the supporting base is not considered. Different oscillation patterns of the model are illustrated in Fig. 2.

## 4. Mathematical Near-Fault Pulse Models

To study the response of structure to near-fault pulses with different periods, artificial ground motions have been used. For this purpose, regarding the fact that directivity and fling pulses have a relatively deterministic nature, some

researchers tried to present synthetic models for these pulse-type motions (for example, [27–33]). In this study, the model proposed by Mavroeidis and Papageorgiou [34] has been used to mathematically express the directivity pulse. The mathematical equation of its velocity record is as follows:

$$v(t) = A\frac{1}{2}\left[1+\cos\left(\frac{2\pi\cdot f_p}{\gamma}\left(t-t_0\right)\right)\right]\cos\left[2\pi\cdot f_p\left(t-t_0\right)+\nu\right] \quad (1)$$

$$\text{for } t_0-\frac{\gamma}{2f_p}\le t\le t_0+\frac{\gamma}{2f_p}$$

where $A$, $f_p$, $\gamma$, and $\nu$ indicate pulse amplitude, prevailing pulse frequency, the number of cycles, and phase, in the same order.

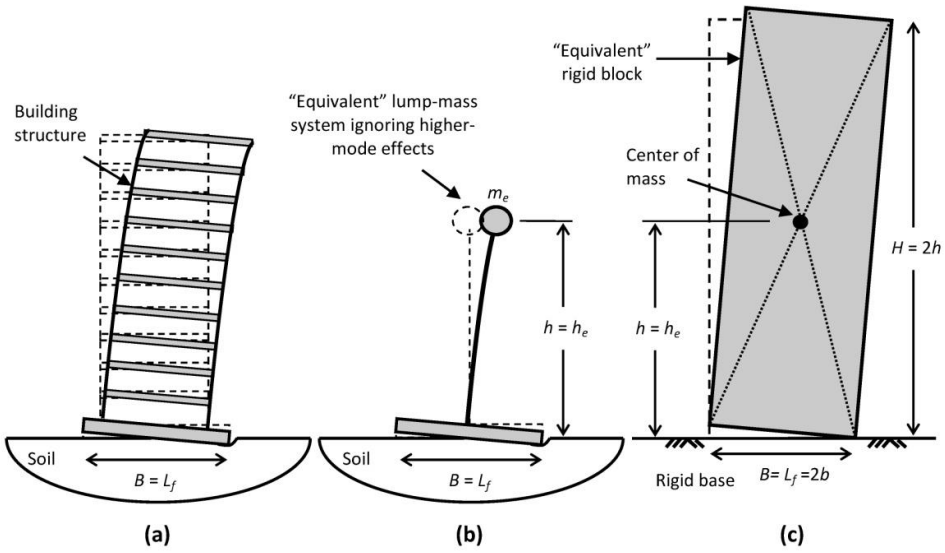


**Fig. 1:** The analogy between the rocking response of a building structure and equivalent rigid block subjected to base excitation.

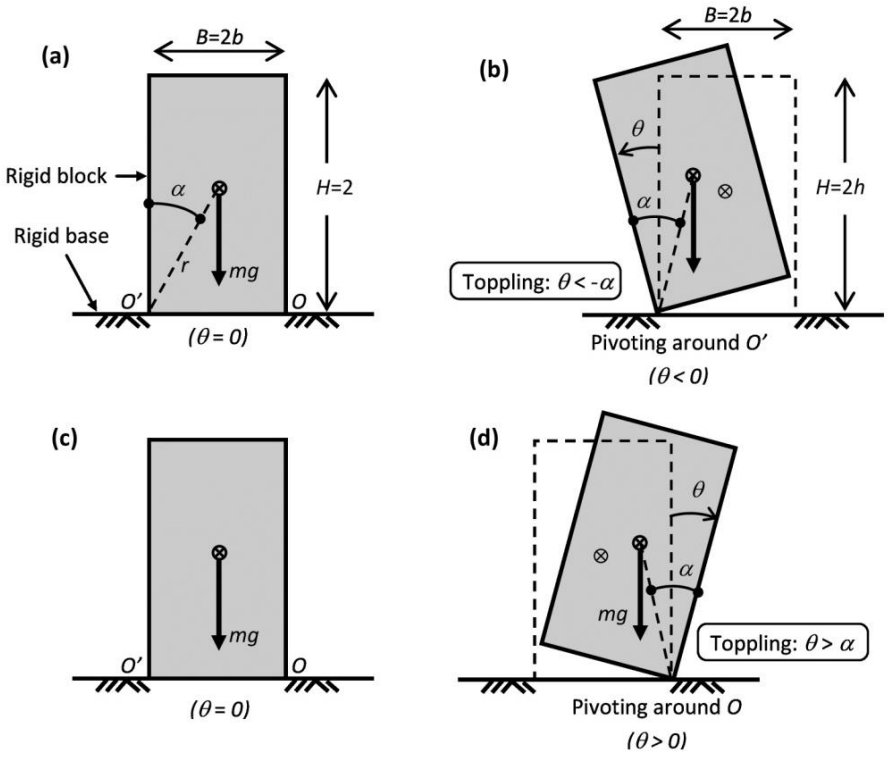


**Fig. 2:** Sequential states of the rigid block on rigid base: a) at rest; b) negative rocking ($\theta(t) < 0$); c) impact condition ($\theta(t) = 0$); d) positive rocking ($\theta(t) > 0$).

The $t_0$ shows the time of pulse arrival, and $\gamma$ is a number between 1 and 3, which is chosen as 2 in this study. $\nu$ is used for better fitness of pulse on real record, and in this study, its value is zero.

For different records, $A$ has a value close to the record's Peak Ground Velocity (PGV). Several equations based on magnitude and distance are presented for PGV (e.g. Alavi and Krawinkler [28]; Bray and Rodriguez-Marek [27]; Xin-le and Xi [35]). Since $A$ is related to rise velocity in the fault, and since rise velocity is equal to the ratio of rising displacement to rise time and both of them are functions of rupture specified length, hence $A$ is independent of rupture specified length and, as a consequence, independent of magnitude, and as an approximation, a value of 100 cm/s is chosen as pulse amplitude [34].

Another parameter used as a control variable in this paper is the pulse period ($T_p$), which is the inverse of prevailing pulse frequency ($f_p$). This parameter is a function of rising time and is in direct relation with magnitude. Several equations are presented for the relation of pulse period and magnitude [6,27,28,34,35].

The proposed relation by Mavroeidis and Papageorgiou [34] is:

$$log\, T_p = -2.9 + 0.5M_w \tag{2}$$

In which $T_p$ is in second and $M_w$ shows the magnitude. Since the mainspring of this study is to evaluate the effect of $T_p$ variations, a wide range of 0.5-3.0 s with steps of 0.25, and 3.0-5.0 s with steps of 0.5, and then 5.0-12.5 s with steps of 2.5 is considered. According to Equation (2), the entire range of $T_p$ used in this study with lower and upper bound equal to 0.5 and 12.5 s corresponds with magnitude ($M_w$) of 4.4 and 7.2, respectively.

The fling pulse used in this study is based on the model proposed by Sasani and Bertero [29]. The mathematical equation of its acceleration record is as follows:

$$a(t) = \frac{2\pi D}{T_p{}^2}\sin\left[\frac{2\pi}{T_p}(t - T_i)\right], \quad \text{for} \quad T_i \le t \le T_i + T_p \tag{3}$$

Where, $D$ denotes the residual ground offset at the end of pulse duration, and $T_p$ and $T_i$ denote pulse period and pulse arrival time, respectively. The range of $T_p$ variations in this paper is the same as directivity pulse.

## 5. Superstructure

Inasmuch as soil-structure interaction may be considered to affect only the contribution of the fundamental mode of the superstructure (ATC), modal analysis is carried out to incorporate first-mode structural behavior in this study. Based on the modal analysis of the fixed-base superstructure, the effective mass ($m_e$) of the superstructure at $j$th mode is defined by Equation (4).

$$m_e = \frac{\left[\sum_{i=1}^{n} m_i \cdot \varphi_{ij}\right]^2}{\sum_{i=1}^{n} m_i \cdot \varphi_{ij}{}^2} \tag{4}$$

in which $\varphi_{ij}$ should be interpreted as the displacement amplitude of the $i$th floor when the structure is vibrating in its fixed-base fundamental natural mode (i.e. $j$=1), and $m_i$ is the seismic mass at $i$th level of the $n$-story building. The effective height ($h_e$) of the superstructure is also defined by Equation (5).

$$h_e = \frac{\sum_{i=1}^{n} m_i \cdot \varphi_{i1} \cdot h_i}{\sum_{i=1}^{n} m_i \cdot \varphi_{i1}} \tag{5}$$

in which $\varphi_{i1}$ has the same meaning as the quantity $\varphi_{i1}$ in Equation (4) when $j$=1. In the interest of simplicity, it is recommended by ATC as a good approximation to assume linear fundamental natural mode shape for typical tall buildings for which the weight is uniformly distributed along with the height. On the other hand, according to Bielak (1969), who investigated the response of fixed-base systems, the contributions of the second and higher modes to the overturning moment at the base of any classical linear system whose fundamental mode is given by a straight line, vanish identically. Hence, such a mode shape which increases linearly from the base to the top of the building is used in this study to calculate $\varphi_{i1}$ quantities in Equations (4-5). Accordingly, for 10-, 15-, and 20-story buildings that are investigated in this paper, the first-mode mass participation factors obtained are equal to 0.786, 0.774, and 0.768, respectively. The effective height ($h_e$) obtained is also equal to 70% of the total height of the buildings.

In terms of higher-mode effects, it is noted that the current codes of practice, such as the International Building Code [36], require to consider all significant modes, so that at least 90 percent of the participating mass of the structure is included in the calculation of response. However, due to the fact that only the fundamental mode has a nonvanishing base moment and therefore, a tendency to rotate [37], the rotation of the base does not occur in the higher modes under these circumstances. As a result, the higher-mode effects can be reasonably ignored for the purpose of overturning analysis.

## 6. Parametric Study

To make a reliable assessment of nonlinear SSI effects on seismic performance of rocking structures subjected to near-fault pulses, it is extremely important to choose a combination of different sets of parameters appropriately. These sets of parameters are (i) ground motion characteristics that have been studied in section 4, (ii) structural properties of the superstructure, and (iii) foundation design parameters.

The second set of parameters describing the structural properties of the buildings are presented in Table 1. These parameters are calculated according to the modal approach explained in section 5 for 10-, 15-, and 20-story buildings with a geometric aspect ratio (or slenderness ratio, *SR*) of 2 and 3. It is noted that since the design of shallow raft foundations for medium-to-high rise buildings with high slenderness is not practical, relatively low values of aspect ratio are selected in this study.

The third set of parameters describing the structural properties of the foundation are presented in Table 2. It is assumed that the superstructure is supported by shallow foundation with no embedment. The raft foundations are designed based on the load bearing capacity of the underlying soil as well as settlement criteria based on recommendations of FEMA P-751 [38]. The vertical static safety factor of foundation ($FS_v$) is a key parameter controlling the potential of foundation uplifting and soil plasticity during foundation-soil interactions. Low values of $FS_v$ means statically heavily-loaded foundations that can exhibit a significant level of nonlinearities during seismic loading. It is noted that geotechnical properties of the subsoil corresponding to soil type B, represents a very dense and rock site according to site classification introduced in ASCE7 [39]. A list of geotechnical properties of the subsoil is presented in Table 3.

## 7. Equation of Motion

When subjected to ground acceleration, $\ddot{x}_g$ , the rigid block will oscillate in the rotational direction with a rocking angle of $\theta(t)$ about corner O ($\theta(t) > 0$) or corner O' ($\theta(t) < 0$) relative to the rigid base.

The single equation of motion of the system in the pure-rotation oscillation pattern is given by:

$$\begin{aligned}&\left(mr^2+I\right)\cdot\ddot{\theta}+mg\left[\operatorname{sgn}\theta\cdot\left(b\cos\theta\right)-h\sin\theta\right]=\\&-m\left[h\cos\theta+\operatorname{sgn}\theta\cdot\left(b\sin\theta\right)\right]\cdot\ddot{x}_g\end{aligned} \tag{6}$$

in which $\theta(t)$ is the angular rotation of the block (positive in the clockwise direction) and sgn($\theta$) is the signum function in $\theta$. Also, $m$ and $I$ are the mass and centroid mass moment of inertia, $I = m\,(h^2+b^2)/3$, for rectangular rigid block, and $r$ denotes half-diameter of the block.

**Table 1:** Structural properties of the building models including fundamental mode of fixed-base superstructure

| No. story | Aspect ratio, *SR* | Weight, $W_{str}$ (kN) | Effective mass, $m_e$ (ton) | Effective height, $h_e$ (m) |
|---|---|---|---|---|
| 10 | 2 | 5883.6 | 388.9 | 21 |
| | 3 | 3922.4 | 259.3 | 21 |
| 15 | 2 | 13238.1 | 862.3 | 31 |
| | 3 | 8825.4 | 574.8 | 31 |
| 20 | 2 | 23534.4 | 1521.2 | 41 |
| | 3 | 15689.6 | 1014.1 | 41 |

**Table 2:** Structural properties of raft foundations with no embedment

| Building aspect ratio, *SR* | 2 | 3 |
|---|---|---|
| Soil type | B | B |
| | 10-story building ($T_f$ = 1.2 m) † | |
| Foundation length, $L_f$ (m) | 15 | 10 |
| Vertical static safety factor of foundation, $FS_v$ | 3.864 | 3.864 |
| Foundation-to-structure weight ratio, $W_f/W_{str}$ | 0.33 | 0.33 |
| | 15-story building ($T_f$ = 1.5 m) | |
| $L_f$ (m) | 22.5 | 15 |
| $FS_v$ | 2.809 | 2.809 |
| $W_f/W_{str}$ | 0.275 | 0.275 |
| | 20-story building ($T_f$ = 1.8 m) | |
| $L_f$ (m) | 34 | 23 |
| $FS_v$ | 2.724 | 2.790 |
| $W_f/W_{str}$ | 0.318 | 0.327 |

† $T_f$ denotes thickness of the foundation

**Table 3:** Geotechnical properties of the underlying soil

| Soil Type | B |
|---|---|
| Density, $\rho$ (t/m$^3$) | 21 |
| Shear modulus, $G$ (MPa) | 130 |
| Poisson's ratio, $\nu$ | 0.35 |
| Cohesion, $C$ (kPa) | 10 |
| Friction angle, $\phi$ (deg) | 40 |
| Shear wave velocity, $V_s$ (m/s) | 800 |

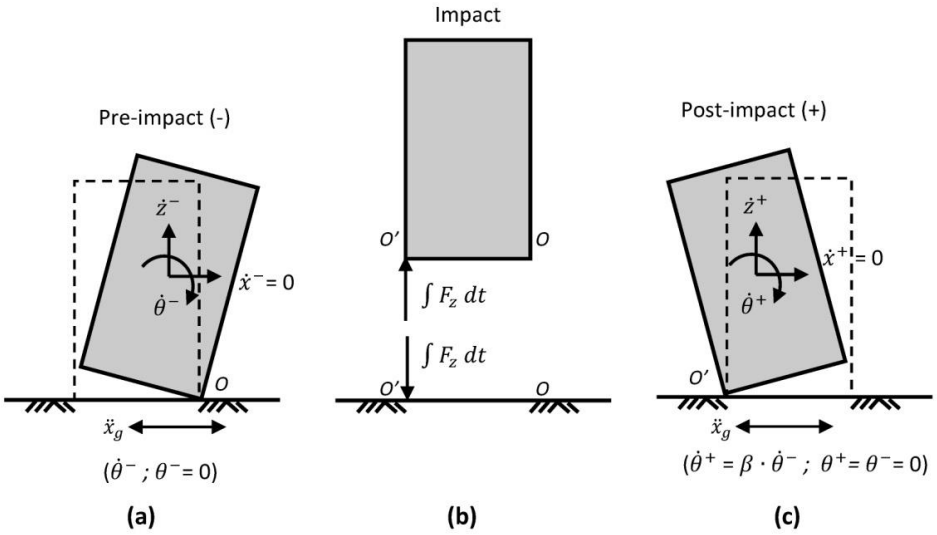


**Fig. 3:** Three consecutive snapshots of the rigid block in: a) pre-impact; b) impact; c) post-impact condition. Rocking about corner O is followed by re-uplifting about O'.

Evidently, the equation of motion governing the rocking regime is highly nonlinear and not amenable to closed-form solution, even for the simplest form of ground excitation. The signum function in $\theta$ is used in Equation (6) in order to represent the equation of motion in two different phases, namely positive and negative rocking, as displayed in Figs. 2c and 2a, respectively. Note that Equation (6) holds only in the absence of impact ($\theta \neq 0$). At that instant, both corner points O and O' are in contact with the base, rendering the above formulation invalid.

To overcome this problem, the subsequent instants at which impact occurs are deinterlaced during the time-domain analysis of Equation (6). Impact condition takes place when the rigid block is switching from one oscillation pattern to another (see Fig. 3). In such a condition, time-domain integration of equation of motion at the end of the pre-impact phase (Fig. 3a) terminates. Then analytical force-based formulation is carried out in order to impose the effect of the impact problem. Next, the integration of equation of motion governing the post-impact phase (Fig. 3c) must account for the ensuing instantaneous change of the system's velocity. The detailed formulation of impact problem is addressed in the following.

## 8. Impact Problem

The dynamic response of the system is strongly affected by the occurrence of impacts between the block and the horizontally-moving base. In fact, it renders the problem nonlinear by virtue of the discontinuity introduced in the response. The impact causes the system to switch from one oscillation phase to another i.e. from positive to negative rocking and vice versa (see Fig. 2).

The critical role of impact on the dynamics of the system necessitates a rigorous formulation of the impact problem. A model governing impact is derived herein using classical impact theory. According to the principle of impulse and momentum, the duration of impact is assumed short, and the impulsive forces are assumed large, relative to other forces in the system. Changes in position and orientation are neglected, and changes in velocity are considered instantaneous. Moreover, this model assumes a point-impact, zero coefficient of restitution (perfectly inelastic impact), impulses acting only at the impacting corner (impulses at the rotating corner are small compared to those at the impacting corner and are neglected), and sufficient friction to prevent sliding of the block during impact. The assumptions made in solving the impact problem are similar to those of Roussis and Odysseos [40] for dynamic analysis

of seismically isolated rigid blocks subjected to near-fault ground motions.

Under the assumption of perfectly inelastic impact, the only possible response mechanism of the following impact would be rocking about the impacting corner when the block re-uplifts (no bouncing), i.e. switching from positive to negative rocking or vice versa (see Fig. 2). The formulation of impact is divided into three phases: pre-impact, impact, and post-impact, as illustrated schematically in Fig. 3. In the following notation, the superscript "-" refers to a pre-impact quantity and superscript "+" to a post-impact quantity. As stated before, it is assumed that impact is accompanied by an instantaneous change in velocities, while the system displacements remain unchanged during the impact phase (Fig. 3b). Hence, the impact analysis is reduced to the calculation of initial conditions for the post-impact motion, $\dot{\theta}^{+}$, given the position ($\theta = 0$) and the pre-impact velocity, $\dot{\theta}^{-}$.

The principle of linear impulse and momentum for the rigid block at impact phase (Fig. 3b) along the vertical direction (z-axis) states that

$$\int F_z dt = m\dot{z}^{+} - m\dot{z}^{-} \tag{7}$$

in which $\int F_z dt$, $\dot{z}^{-}$ and $\dot{z}^{+}$ are the vertical impulse (assumed to be applied at O') and the absolute pre- and post-impact vertical velocities of the mass center of the block, respectively. In addition, the principle of angular impulse and momentum states that

$$b \cdot \left( \int F_z dt \right) = I\dot{\theta}^{+} - I\dot{\theta}^{-} \tag{8}$$

In Equation (7), the pre- and post-impact vertical components of the relative translational velocity of the mass center can be expressed in terms of the angular velocity of the block as

$$\dot{z}^{-} = b\dot{\theta}^{-}, \quad \dot{z}^{+} = -b\dot{\theta}^{+} \tag{9}$$

Substituting Equation (9) into Equation (7) yields:

$$\int F_z dt = -mb\dot{\theta}^{+} - mb\dot{\theta}^{-} \tag{10}$$

Equations (8) and (10) constitute a set of two equations into two unknowns. Equivalently, combining these equations in one equation (by eliminating the vertical impulse) gives the post-impact velocity as:

$$\dot{\theta}^{+} = \frac{h^2 - 2b^2}{h^2 + 4b^2} \cdot \dot{\theta}^{-} = \beta \cdot \dot{\theta}^{-} \tag{11}$$

or

$$\dot{\theta}^{+} = \frac{SR^2 - 2}{SR^2 + 4} \cdot \dot{\theta}^{-} \tag{12}$$

where *SR* denotes geometric aspect ratio of the rigid block. So far, according to the impact analysis, the initial conditions for the post-impact motion, $\dot{\theta}^{+}$, given the position ($\theta = 0$) and the pre-impact velocity, $\dot{\theta}^{-}$, is calculated.

## 9. Numerical Results

The numerical integration of the equation of motion is performed using a step-by-step formulation. This way the geometric nonlinear behavior of Equation (6) may be simulated using linear dynamic models. The basic idea is that the loading and the response history are divided into a sequence of time intervals or "steps". By assuming that the system properties remain constant during each step, any desired degree of refinement in the nonlinear behavior may be achieved by making the time steps short enough. This procedure can be applied to any type of nonlinearity, including geometric nonlinearity. In more precise words, the trigonometric functions in $\theta$ in Equation (6) can be approximated by first-order polynomials, and this linearization will give rise to the classical equation of motion during each step. The simplest step-by-step method for analysis of sdof systems is the so-called "piecewise exact" method. This method is based on the exact solution of the equation of motion for the response of a linear structure to a loading that varies linearly during a discrete-time interval [41]. The piecewise exact method has been executed in Matlab [42] for numerical integration of the equation of motion.

As an example, the system's response to a given directivity as well as fling pulse is presented in Fig. 4. Results are presented here for a system of a homogeneous rigid block with a height of $H=2h$ and base width of $B=2b$. These blocks are representative of the first-mode equivalent sdof model of the 10-, 15-, and 20-story structures with an aspect ratio of 2 and 3 as introduced in Table 1 (see Fig. 1). The foundation design parameters are presented in Table 2.

The results of Fig. 4 depict a comparison of the computed response in terms of the rotation histories of the equivalent rigid blocks. It is noteworthy that structural flexibility, including elastic as well as inelastic deflections, is ignored in this study. To explain, rocking instability of the superstructure stems from rigid-body rotation around the corner of its foundation, and that is why the structural deformations are not of primary importance while overturning resistance is being analyzed. In this circumstance, the sdof system undergoes large displacement (i.e. large rotation) prior to toppling initiation which is an order of magnitude greater than small structural displacements. For instance, as shown in Figure 4, in case of the 10-story building with a slenderness ratio (SR) of 3 subjected to fling pulse, θ has reached 0.25 rad while toppling was initiated, which accounts for a considerably large rotation.

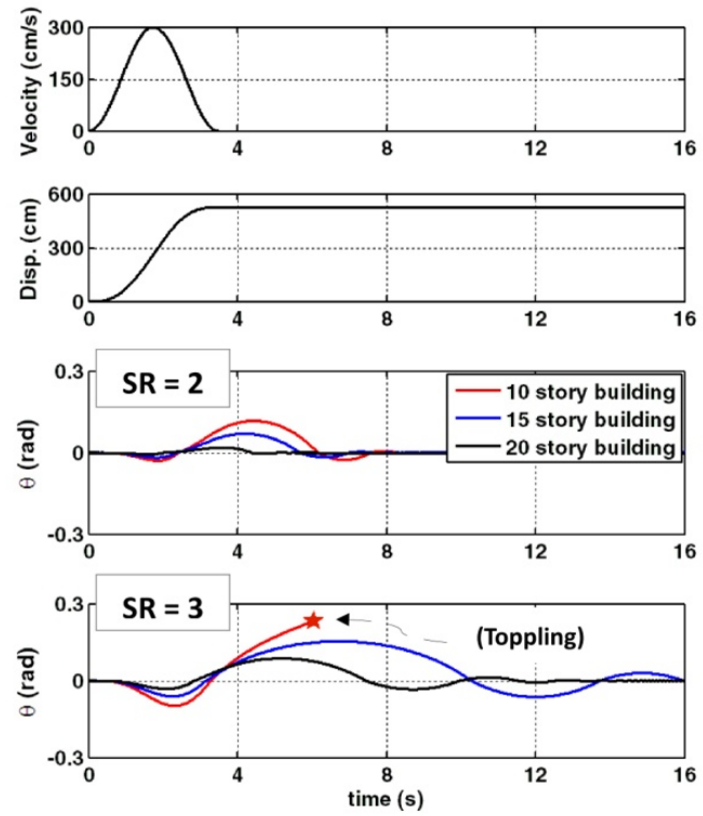


(a) Fling pulse

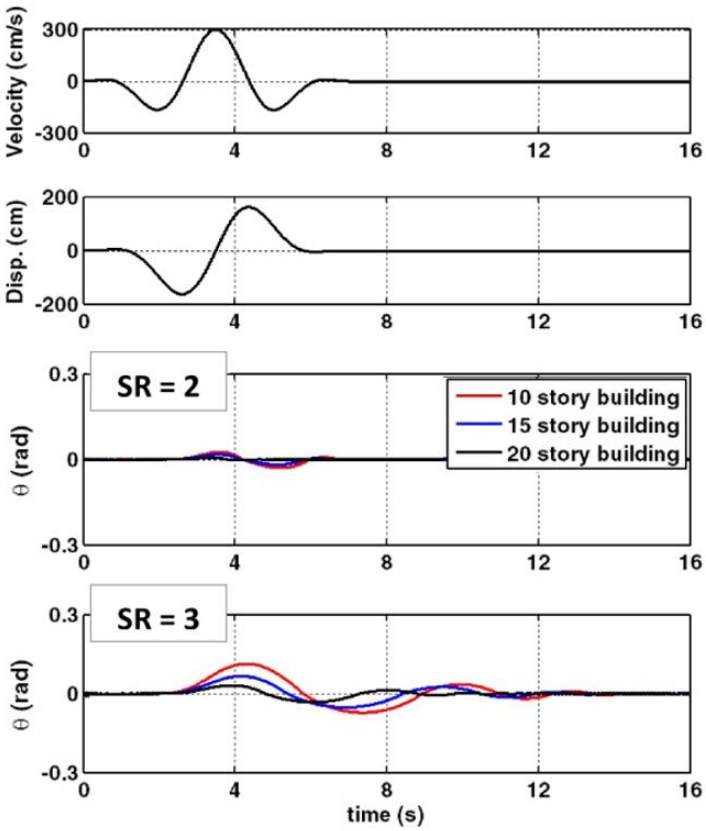


(b) Directivity pulse

**Fig. 4:** Rotation response histories of the equivalent rigid blocks to directivity as well as fling pulse.

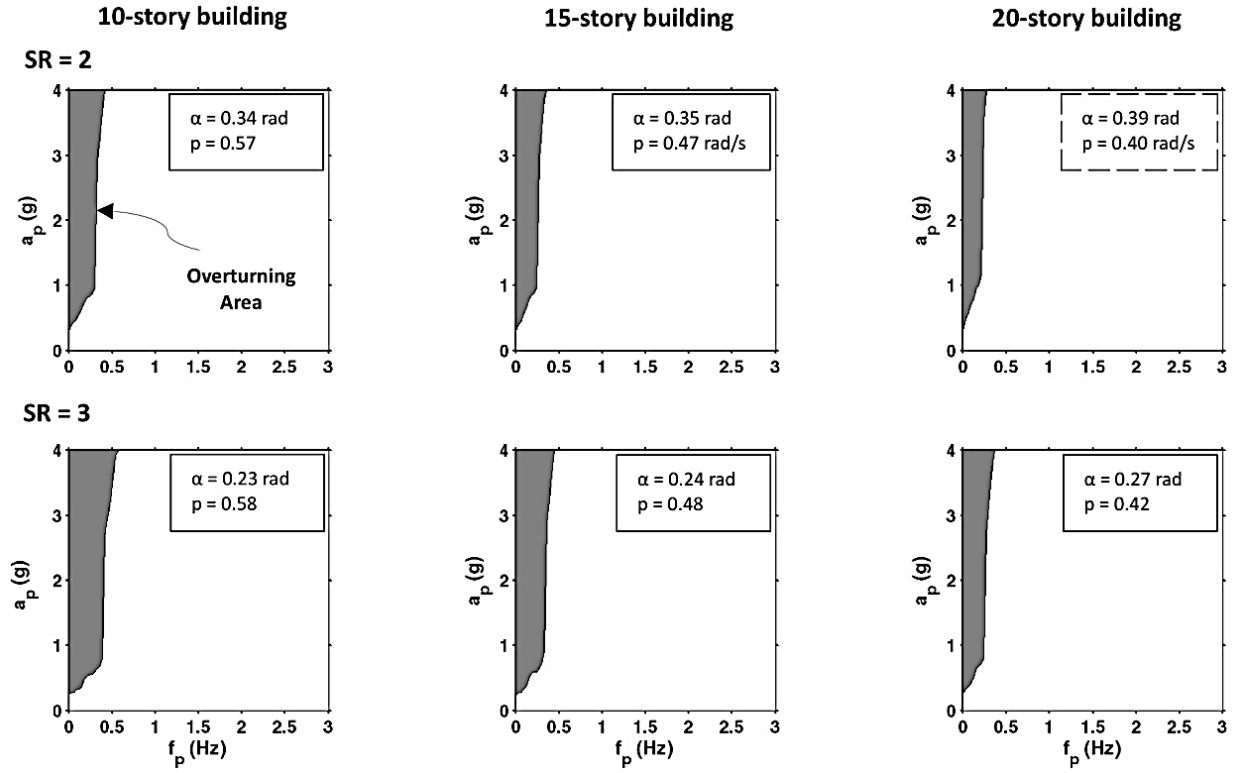


**Fig. 5:** Overturning spectra of the equivalent rigid blocks subjected to "directivity" pulses (The shaded areas represent unsafe regions within which overturning would occur).

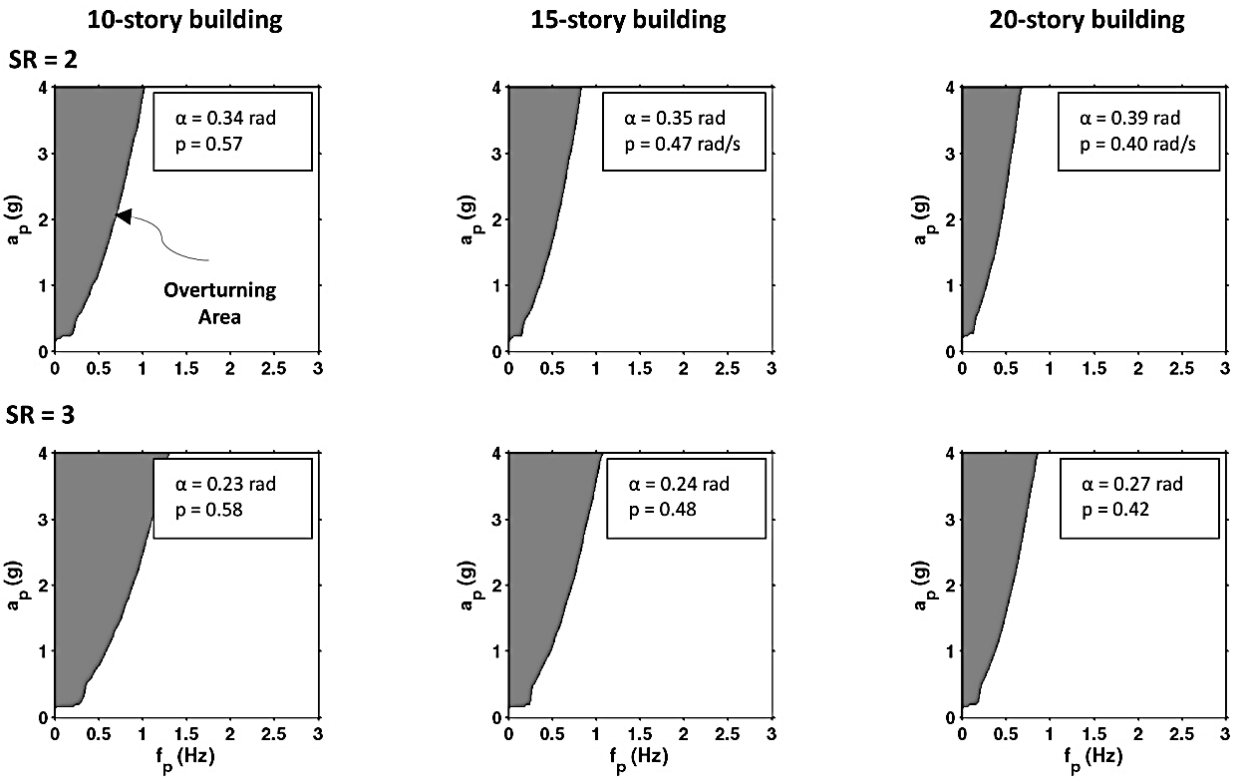


**Fig. 6:** Overturning spectra of the equivalent rigid blocks subjected to "fling" pulses (The shaded areas represent unsafe regions within which overturning would occur).

It can be observed that the rocking response of rigid blocks is greater under base excitation of fling pulse compared to the directivity pulse of the same amplitude. So, the model of a 10-story building with an aspect ratio of 3 topples under fling pulse excitation ($\theta > \alpha$). Moreover, the intensity of the blocks' rocking response decreases when the geometrical size of the buildings increases. This observation is in compliance with the so-called scale effect which was proposed by Housner [43] for the first time, which makes the larger of two geometrically similar blocks more stable than the smaller block. Accordingly, he concluded that the survival against the toppling of such large-size slender structures during earthquakes is not surprising.

The results also confirm that slender blocks are more rocking dominated and consequently more prone to overturning instability compared to squat blocks.

To assess the overturning potential of the buildings subjected to near-fault pulses quantitatively, a variety of mathematical directivity and fling pulses of different prevalent pulse frequency ($f_p$) and acceleration pulse amplitude ($a_p$) are investigated. The results of this parametric study are summarized in the form of behavior maps in Figs. 5 and 6 for 10-, 15-, and 20-story buildings with an aspect ratio of 2 and 3 subjected to directivity and fling pulses.

Dealing with the results of Figs. 5 and 6, it is noted that a rigid block of width $B$=2$b$ and height $H$=2$h$ (Fig. 2b) is characterized by its ultimate reversible angle of rotation $\alpha$

$$\alpha = \tan^{-1}\left(b/h\right) \tag{13}$$

and the frequency parameter $p$

$$p = \sqrt{3g/4r} \tag{14}$$

in which $g$ and $r$ denote the acceleration of gravity and half-diameter of the block, respectively [44]. The latter can be seen as a measure of the dynamic characteristics of the block and decreases with the size of the block. Both of the characteristic parameters are given for each block in Figs. 5 and 6.

A total of 10,000 nonlinear dynamic analyses are performed in constructing each overturning spectrum in Figs. 5 and 6. In each overturning spectrum, the shaded area indicates an "unsafe region" within which the overturning instability occurs. Comparing the overturning spectra of Fig. 5 with those of Fig. 6 reveals that fling pulses are more destructive than directivity pulses of the same magnitude with respect to overturning potential. This observation can be interpreted by the inherent one-sided pattern of excitation in the velocity history of fling pulses compared to a double-sided pattern in directivity pulses.

The overturning spectra in Figs. 5 and 6 also confirm that slender blocks (i.e. with greater aspect ratio) are more capable of toppling than squat blocks. On the other hand, it is observed that the shaded area, within which the rocking superstructure could not survive, is narrowed when the geometric size of the building increases. Narrow unsafe regions in more large-size buildings can be explained by the key frequency parameter ($p$) which controls the level of rocking domination during a given base shaking. Evidently, lower frequency parameter ($p$) of the more large-size buildings is a quantity that indicates higher safety margins against toppling. This so-called scale effect was firstly proposed by Housner [43].

## 10. Conclusions

Seismic performance of rocking soil-structure systems subjected to near-fault pulses, including foundation uplifting, is focused in this paper. To this end, an extensive parametric study is conducted. Medium-to-high-rise building structures with different aspect ratios based on shallow raft foundation locations are investigated. Mathematical directivity and fling pulses are used as input ground motion. The overturning potential is investigated when the rocking structure is subjected to directivity and fling pulses. The major findings of this paper are outlined in the following.

Two-dimensional overturning spectra of buildings of various geometrical, as well as dynamic characteristics, are derived. It was observed that the prevalent pulse period ($T_p$) is a key parameter governing the overturning potential. As another conclusion, fling pulses are more destructive than directivity pulses of the same magnitude with respect to overturning potential. This observation can be interpreted by the inherent one-sided pattern of excitation in the velocity history of fling pulses compared to a double-sided pattern in directivity pulses. Evidently, the lower frequency parameter ($p$) of the more large-size buildings is a quantity that indicates higher safety margins against toppling.

## References


**[1]** Somerville P. Seismic hazard evaluation. Bull New Zeal Soc Earthq Eng 2000;33:371–86.

**[2]** Abrahamson N. Incorporating effects of near fault tectonic deformation into design ground motions. A Present Spons by EERI Visit Prof Program, Hosted by Univ Buffalo 2001.

**[3]** Chen X, Liu Y, Zhou B, Yang D. Seismic response analysis of intake tower structure under near-fault ground motions with forward-directivity and fling-step effects. Soil Dyn Earthq Eng 2020;132:106098.

**[4]** Bertero V V, Herrera RA, Mahin SA. Establishment of design earthquakes—Evaluation of present methods. Proc., Int. Symp. Earthq. Struct. Eng., vol. 1, Univ. of Missouri-Rolla Rolla, Mo.; 1976, p. 551–80.

**[5]** Iwan WD, Huang C-T, Guyader AC. Important features of the response of inelastic structures to near-field ground motion. Proc. 12th World Conf. Earthq. Eng., 2000.

**[6]** Masaeli H, Khoshnoudian F, Ziaei R. Rocking soil-structure

systems subjected to near-fault pulses. J Earthq Eng 2015;19:461–79.
**[7]** Jangid RS, Kelly JM. Base isolation for near- fault motions. Earthq Eng Struct Dyn 2001;30:691–707.
**[8]** Pavlou EA, Constantinou MC. Response of elastic and inelastic structures with damping systems to near-field and soft-soil ground motions. Eng Struct 2004;26:1217–30.
**[9]** Mavroeidis GP, Dong G, Papageorgiou AS. Near- fault ground motions, and the response of elastic and inelastic single- degree-of- freedom (SDOF) systems. Earthq Eng Struct Dyn 2004;33:1023–49.
**[10]** Kalkan E, Kunnath SK. Effects of fling step and forward directivity on seismic response of buildings. Earthq Spectra 2006;22:367–90.
[11] Zhai C, Li S, Xie L, Sun Y. Study on inelastic displacement ratio spectra for near-fault pulse-type ground motions. Earthq Eng Eng Vib 2007;6:351–5.
**[12]** Yalcin OF, Dicleli M. Effect of the high frequency components of near-fault ground motions on the response of linear and nonlinear SDOF systems: a moving average filtering approach. Soil Dyn Earthq Eng 2020;129:105922.
**[13]** Lu Y, Hajirasouliha I, Marshall AM. Direct displacement-based seismic design of flexible-base structures subjected to pulse-like ground motions. Eng Struct 2018;168:276–89.
**[14]** Spyrakos CC, Nikolettos GS. Overturning stability criteria for flexible structures to earthquakes. J Eng Mech 2005;131:349–58.
**[15]** Zhang J, Tang Y. Dimensional analysis of structures with translating and rocking foundations under near-fault ground motions. Soil Dyn Earthq Eng 2009;29:1330–46.
**[16]** Acikgoz S, DeJong MJ. The interaction of elasticity and rocking in flexible structures allowed to uplift. Earthq Eng Struct Dyn 2012;41:2177–94.
**[17]** Peng W, Zhao H, Dai F, Taciroglu E. Analytical method for overturning limit analysis of single-column pier bridges. J Perform Constr Facil 2017;31:4017007.
**[18]** Haeri SM, Fathi A. Numerical modeling of rocking of shallow foundations subjected to slow cyclic loading with consideration of soil-structure interaction. ArXiv Prepr ArXiv180804492 2018.
**[19]** Jia C, Huang Q, Wang G. Stability analysis of blocky structure system using discontinuity layout optimization. Int J Numer Methods Eng 2020;121:5766–83.
**[20]** Ishiyama Y. Review and discussion on overturning of bodies by earthquake motions 1980.
**[21]** Koh A-S, Spanos PD, Roesset JM. Harmonic rocking of rigid block on flexible foundation. J Eng Mech 1986;112:1165–80.
**[22]** Psycharis IN, Jennings PC. Rocking of slender rigid bodies allowed to uplift. Earthq Eng Struct Dyn 1983;11:57–76.
**[23]** Makris N, Roussos YS. Rocking response of rigid blocks under near-source ground motions. Geotechnique 2000;50:243–62.
**[24]** Gerolymos N, Apostolou M, Gazetas G. Neural network analysis of overturning response under near-fault type excitation. Earthq Eng Eng Vib 2005;4:213.
**[25]** Gelagoti F, Kourkoulis R, Anastasopoulos I, Gazetas G. Rocking-isolated frame structures: Margins of safety against toppling collapse and simplified design approach. Soil Dyn Earthq Eng 2012;32:87–102.
**[26]** Bielak J. Base moment for a class of linear systems. J Eng Mech Div 1969;95:1053–62.
**[27]** Bray JD, Rodriguez-Marek A. Characterization of forward-directivity ground motions in the near-fault region. Soil Dyn Earthq Eng 2004;24:815–28.
**[28]** Alavi B, Krawinkler H. Consideration of near-fault ground motion effects in seismic design. Proc. 12th World Conf. Earthq. Eng., vol. 8, 2000.
**[29]** Sasani M, Bertero V V. Importance of Severe Pulse-Type Ground Motions in Performance-Based Engineering: Historical and Critical. Proc. 12th World Conf. Earthq. Eng. New Zeal. Soc. Earthq. Eng. Up. Hutt, New Zeal., 2000.
**[30]** He W-L, Agrawal AK. Analytical model of ground motion pulses for the design and assessment of seismic protective systems. J Struct Eng 2008;134:1177–88.
**[31]** Xin L, Li X, Zhang Z, Zhao L. Seismic behavior of long-span concrete-filled steel tubular arch bridge subjected to near-fault fling-step motions. Eng Struct 2019;180:148–59.
**[32]** Zengin E, Abrahamson NA. A vector-valued intensity measure for near-fault ground motions. Earthq Eng Struct Dyn 2020;49:716–34.
**[33]** Howard JK, Tracy CA, Burns RG. Comparing observed and predicted directivity in near-source ground motion. Earthq Spectra 2005;21:1063–92.
**[34]** Mavroeidis GP, Papageorgiou AS. A mathematical representation of near-fault ground motions. Bull Seismol Soc Am 2003;93:1099–131.
**[35]** Li X, Zhu X. Study on equivalent velocity pulse of nearfault ground motions. Acta Seismol Sin 2004;17:697–706.
**[36]** International Code Council. International building code. 2018.
**[37]** Jennings PC, Bielak J. Dynamics of building-soil interaction. Bull Seismol Soc Am 1973;63:9–48.
**[38]** Federal Emergency Management Agency. NEHRP Recommended Seismic Provisions: Design Examples 2012.
**[39]** American Society of Civil Engineers. Minimum design loads for buildings and other structures: second Printing (ASCE/SEI 7). 2010.
**[40]** Roussis PC, Odysseos S. Dynamic response of seismically isolated rigid blocks under near-fault ground motions. Proc. 15th World Conf. Earthq. Eng., 2012.
**[41]** Clough RW, Penzien J. Dynamics of structures. Berkeley. CA Comput Struct 2003.
**[42]** The MathWorks. MATLAB & Statistics Toolbox Release 2012.
**[43]** Housner GW. The behavior of inverted pendulum structures during earthquakes. Bull Seismol Soc Am 1963;53:403–17.
**[44]** Gelagoti F, Kourkoulis R, Anastasopoulos I, Gazetas G. Rocking isolation of low-rise frame structures founded on isolated footings. Earthq Eng Struct Dyn 2012;41:1177–97.